

Experimental and numerical investigation into the damage response of composite sandwich panels to low-velocity impact

Dianshi Feng^{1a} and Francesco Aymerich^{*2}

¹Department of Civil and Environmental Engineering, National University of Singapore,
No.1 Engineering Drive 2, Singapore

²Department of Mechanical, Chemical and Materials Engineering, University of Cagliari,
Via Marengo 2, Cagliari, Italy

(Received February 26, 2017, Revised April 19, 2017, Accepted April 21, 2017)

Abstract. The paper describes the results of an experimental and numerical investigation into the structural and damage response of sandwich composites to low-velocity impact. Sandwich panels consisting of laminated composite skins with three different layups bonded to a PVC foam core were subjected to impact at various energy levels corresponding to barely visible impact damage (BVID) in the impacted skins. Damage assessment analyses were performed on the impacted panels to characterise the extent and the nature of the major failure mechanisms occurring in the skins. The data collected during the experimental analyses were finally used to assess the predictive capabilities of an FE tool recently developed by the authors for detailed simulation of impact damage in composite sandwich panels. Good agreement was observed between experimental results and model predictions in terms of structural response to impact, global extent of damage and typical features of individual damage mechanisms.

Keywords: sandwich composites; low-velocity impact; damage; FE simulation

1. Introduction

Sandwich composite structures made of thin fibre-reinforced composite skins separated by a thick core material of low density are being increasingly adopted for lightweight constructions in a wide range of engineering areas, including the transport, construction and energy sectors.

Because of their high strength and stiffness to weight ratios, good corrosion properties, and flexibility in design options, sandwich composites are particularly attractive materials for use in wind turbine blades, where high bending stiffness and buckling resistance are specifically required in combination with good static and fatigue strength properties (Thomsen 2009).

The technical requirements of materials for wind turbine blades are governed by the following major constraints (Thomsen 2009, Burton *et al.* 2011, Brøndsted and Nijssen 2013), which must be considered to optimize the structural configuration for increased reliability and service life:

- low blade weight is required to reduce gravity loads;
- high material stiffness is required to avoid instability of structural components under

*Corresponding author, Professor, E-mail: francesco.aymerich@dimcm.unica.it

^a Ph.D., Email: ceefd@nus.edu.sg

compression loads and to prevent collision with the tower;

- high static and fatigue strengths are required to resist the extreme and the time-varying loads during the life of the structure, and to reduce material degradation.

Weight, stiffness and buckling properties (both at a local and at a global level), as well as static and fatigue strength performances, are thus the critical design drivers for optimal selection of materials; for these reasons, modern blades are generally made of composite materials, such as glass or carbon fibre reinforced polymers, used in a combination of monolithic (single skin laminates) and sandwich configurations (Hayman *et al.* 2008, Thomsen 2009).

Composite sandwich construction is currently used in many portions of the blades (leading and trailing edges of the wing shells, webs of the main spar, internal stiffeners) to increase the compressive or shear buckling resistance of the structure. More recently, with the development of large wind turbine blades, characterized by the presence of large unstiffened panels that are prone to failure in local buckling, sandwich configurations are also being considered, as an alternative to single skin designs, for potential use in other primary structural elements of the blade, such as the load carrying flange of the main spar or the spar-caps of the wing shells (Berggreen *et al.* 2007, Thomsen 2009).

A major concern in using sandwich composites in primary blade elements is their susceptibility to damage due to impact loading (Abrate 1997). Impacts are often classified in the two classes of low-velocity and high-velocity impacts depending on the response of the structure (Chai and Zhu 2011). High velocity impacts are defined as those impacts in which the contact duration is so short that the response of the structure is dominated by the propagation of through-thickness stress waves, resulting in very localized deformation and damage. In low-velocity impacts, in contrast, the response of the structure is governed by the global deformation of the structure, since the duration of the contact is much longer than the time needed for the stress waves to propagate to the boundary of the structure. As a consequence, low-velocity impacts are especially dangerous since the resulting damage may be difficult – if not impossible- to detect by visual inspection of the material surface (Barely Visible Impact Damage – BVID). Damage mechanisms induced by low-velocity impacts (typically a combination of various failure mechanisms, such as delaminations, matrix cracking, fibre fracture, face-core debonding and core crushing) may lead to severe reductions in stiffness and strength of the sandwich material and result in local failure of the structural element, or even in global collapse of the entire blade.

The loading conditions generally considered in blade design consist of combinations of aerodynamic, gravitational and inertial loads, as well as of loads generated by the actions of the control systems (Burton *et al.* 2011). However, in view of the high vulnerability of composite sandwich materials to impact damage, further load cases associated to typical operational conditions, such as those arising from impacts with hail, birds and foreign objects during operation, or from accidental impacts that inevitably occur during manufacturing, transport, assembly and maintenance (Det Norske Veritas 2002), must also be taken into account at the design stage. While conventional design procedures account for the presence of impact damage by introducing conservative safety or knock-down factors (Det Norske Veritas 2002, Det Norske Veritas 2006), more advanced damage tolerance concepts (Hayman 2007) are being gradually introduced in the design process of critical elements of composite blades, so as to take full advantage of the weight-saving opportunities offered by sandwich materials.

Design schemes based on a damage tolerance approach (Zenkert *et al.* 2005, Ransom *et al.* 2013) assume that damage (either introduced during manufacturing or induced by accidental loads) exists at a critical location and verify that the structure retains the required residual properties in

the presence of the existing damage. In this respect, numerical simulations may provide an efficient alternative, at least at a preliminary or intermediate design phase, to costly experimental tests for assessing the impact response of complex sandwich composite components. Reliable models able to predict nature and extent of damage induced by impact events in composite sandwich elements are thus needed for a safe estimate of residual strength and expected life of the damaged structure and will play a critical role in the successful development of the next generation wind turbine blades.

Only a relatively small number of investigations, typically based on Finite Element (FE) modelling, have been carried out on the prediction of barely visible damage in impacted foam-core sandwich composites. The majority of previous work was based on the use of conventional shell elements and only considered in-ply damage modes, without accounting for delamination between layers, to simulate the damage response of the composite skins (Besant *et al.* 2001, Nguyen *et al.* 2005, Icardi and Ferrero 2009, Mohammed *et al.* 2013, Wang *et al.* 2013). Recently, solid or continuum shell elements were used in a few investigations to model both interlaminar (delamination) and intralaminar damage in composite skins of foam-based sandwich structures subjected to impact or blast (Ivanez *et al.* 2010, Brooks *et al.* 2010, Langdon *et al.* 2013, Yang *et al.* 2015). Stress-based failure criteria together with a sudden stiffness reduction strategy were adopted in (Ivanez *et al.* 2010) to predict the initiation and growth of in-plane and delamination failure modes in the laminated skins of sandwich beam specimens with PVC foam core. Progressive damage models for in-plane fibre and matrix damage, fibre crushing, and delamination between layers, natively available in LS-DYNA, were employed by Brooks and co-workers (Brooks *et al.* 2010) to simulate damage in woven fabric composite skins of sandwich beams. Continuum shell elements implementing progressive degradation of stiffness properties and cohesive elements were used in (Langdon *et al.* 2013, Yang *et al.* 2015) to respectively model individual layers and interfaces between layers in the composite skins of sandwich panels subjected to localized impact or blast loads.

Even though good agreement was generally achieved in these studies between measured and predicted force-time and force-displacement curves, no detailed comparison was provided between experimental and numerical results in terms of size, shape and features of impact-induced damage. In particular, there is still a lack of systematic measurements and observations that could provide a reliable basis of experimental data to assess the accuracy of FE models for prediction of impact damage in sandwich composites with different configurations.

An FE tool adopting energy-based interface cohesive and continuum damage models was recently developed by the authors to predict the structural and damage response of foam-based sandwich composites (Feng and Aymerich 2013). In order to validate the quality of predictions of the proposed FE model, an extensive series of experimental observations and analyses were carried out on sandwich composites consisting of a PVC foam core bonded to carbon/epoxy skins with three different layouts. Experimental data, obtained by low-velocity impact tests and subsequent damage evaluation analyses, were compared with the results of FE simulations for assessing the capabilities of the proposed FE tool to correctly predict size, shape and through-thickness distribution of individual failure modes occurring in the impacted composite skins.

2. Experimental

2.1 Manufacturing of sandwich panels

Sandwich panels with three different skin layups ($[0/90_3/0]$, $[0_4/\pm 45/0_4]$ and $[0_3/\pm 45]_s$) were manufactured and tested to assess the predictive capabilities of the FE simulations in the presence of different impact damage scenarios.

The layups differ in thickness (about 1.6 mm for $[0/90_3/0]$ skins and 3.2 mm for $[0_4/\pm 45/0_4]$, and $[0_3/\pm 45]_s$ skins), and with respect to the number of interfaces prone to delaminations (respectively 2, 3 and 4, in the $[0/90_3/0]$, $[0_4/\pm 45/0_4]$ and $[0_3/\pm 45]_s$ skins). These differences result in dissimilar damage patterns in terms not only of global size, but also of morphology, individual features of failure mechanisms and level of damage complexity, thus providing a series of test-cases for validation of the proposed FE tool.

The composite skins were made with unidirectional carbon/epoxy prepreg layers stacked to achieve desired layups. The prepreg materials was Seal Texipreg[®] HS300/ET223, suitable for vacuum-bag-only processing at curing temperatures ranging between 85°C and 125°C. Individual plies have a fibre volume ratio of 0.62 and a nominal thickness of 0.32 mm. The core material was a Divynicell[®] HP60 PVC foam, which is an elevated temperature foam core grade, with a nominal density of 65 kg/m³, specifically developed for compatibility with low-medium temperature prepreg systems.

The sandwich plates were consolidated in a vacuum-bag using a co-curing process, by simultaneously curing and bonding the prepreg layers to the foam core without the use of additional adhesive material. The curing cycle consisted of a 3°C/min heating stage, followed by a 6 h dwell at 100°C and a cooling stage to room temperature maintaining vacuum. Sandwich panels 250 mm x 250 mm in size with a core thickness of 10 mm were manufactured and tested in the study.

2.2 Impact testing and damage assessment

Impact tests were conducted using an instrumented drop-weight testing machine equipped with a 2.34 kg impactor provided with a hemispherically ended rod of 12.5 mm in diameter (Fig. 1). The panels were impacted with energies ranging between approximately 1 J and 9 J, obtained by varying the drop height of the impactor, and corresponding to impact velocities in the range 0.95-2.8 m/s. It is worth remarking that striking energies up to about 8 J are suggested by the DNV design guidelines to characterize the impact damage resistance in wind turbine blades (Det Norske Veritas 2006). During impact, the sandwich panels were simply supported on a steel plate with a rectangular opening 45 mm x 67.5 mm in size. Impact durations recorded in the experiments ranged between 3 ms and 5 ms, as compared to an estimated time needed for the stress waves to reach the boundary of the samples in the order of tens of μ s (Chai and Zhu 2011). The examined impact events may be therefore classified as low-velocity impacts, according to the definition provided in the introduction.

A series of preliminary tests were also performed to characterize the values of the elastic, strength and fracture properties of the prepreg and foam materials. All tests were performed at room temperature. Internal damage was mainly assessed by penetrant-enhanced X-radiography of the impacted composite skin. In selected samples the through-thickness distribution of impact-inflicted damage was further assessed by stereoscopic X-radiography, ultrasonic

C-scanning and optical microscopy of polished cross-sections.

3. Numerical simulation procedure

3.1 Intralaminar and interlaminar damage models

Energy-based continuum damage mechanics models were adopted for prediction of intralaminar damage in the laminated skins. The intralaminar damage models implemented in the FE analyses are based on the assumptions that the damage process is smeared over the element dimension and that the degradation of the material may be described by a set of internal damage variables d_{ij} that quantify the level of damage sustained by the material (Donadon *et al.* 2008, Falzon and Apruzzese 2011). Stress/strain based initiation criteria and fracture energy based evolution laws were defined for fibre or matrix damage modes. A shear damage model based on the nonlinear response measured under in-plane shear loading on composite layers was also included in the FE analyses. Only a brief summary of the failure models will be provided in this section; a more detailed description of the damage models implemented in the FE analyses was given in (Feng and Aymerich 2013, 2014).

The following criteria were used to identify damage initiation and evolution for tensile or compressive fibre damage

$$F'_{11}(\varepsilon_{11}) = \left(\frac{\varepsilon_{11}}{\varepsilon_{11}^{0r}} \right)^2 - 1 \geq 0 \quad d'_{11}(\varepsilon_{11}) = \frac{\varepsilon_{11}^{ft}(\varepsilon_{11} - \varepsilon_{11}^{0r})}{\varepsilon_{11}(\varepsilon_{11}^{ft} - \varepsilon_{11}^{0r})} \quad \text{Tensile fibre damage} \quad (1)$$

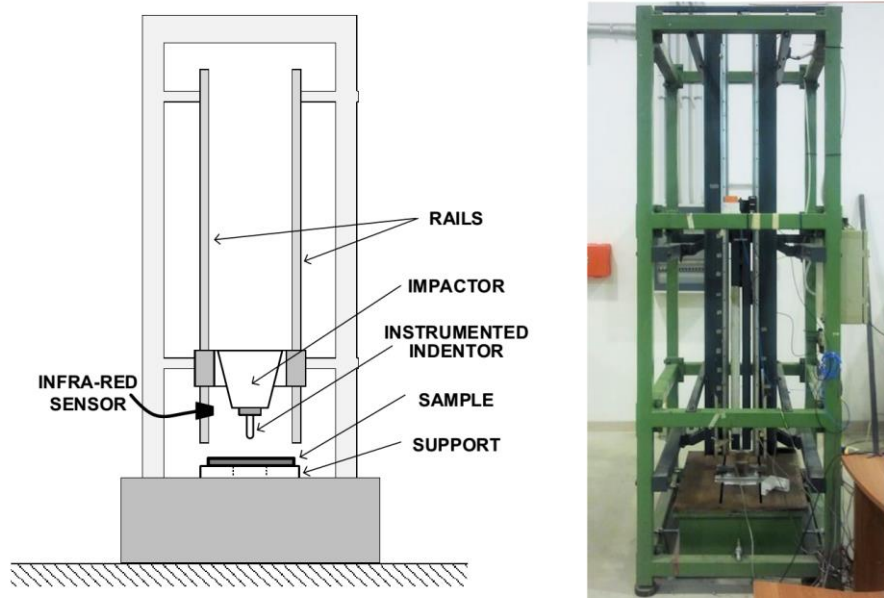


Fig. 1 Drop-weight testing machine used for impact testing

$$F_{11}^c(\varepsilon_{11}) = \left(\frac{\varepsilon_{11}}{\varepsilon_{11}^{0c}} \right)^2 - 1 \geq 0 \quad d_{11}^c(\varepsilon_{11}) = \frac{\varepsilon_{11}^{fc}(\varepsilon_{11} - \varepsilon_{11}^{0c})}{\varepsilon_{11}(\varepsilon_{11}^{fc} - \varepsilon_{11}^{0c})} \quad \text{Compressive fibre damage} \quad (2)$$

A minimum residual value equal to the matrix compressive strength was assigned to the normal compressive strength along the fibre direction in order to account for the interaction of crushed material under compression loads (Donadon *et al.* 2008).

The damage model for initiation and evolution of matrix damage under tension is summarized in the Eqs. (3)

$$F_{22}^t(\varepsilon_{22}) = \left(\frac{\varepsilon_{22}}{\varepsilon_{22}^{0t}} \right)^2 - 1 \geq 0 \quad d_{22}^t(\varepsilon_{22}) = \frac{\varepsilon_{22}^{ft}(\varepsilon_{22} - \varepsilon_{22}^{0t})}{\varepsilon_{22}(\varepsilon_{22}^{ft} - \varepsilon_{22}^{0t})} \quad \text{Tensile matrix damage} \quad (3)$$

while the criterion proposed by Schurmann and Puck (2002), which accounts for the increase of shear strength induced by the presence of a normal compressive stress on the fracture plane, was used for modeling matrix damage under compressive loads. In the above equations, the indices t and c refer to the tensile and compressive response of the lamina, while ε^0 and ε^f represent respectively the strain for failure initiation and the maximum strain for damage parameter equal to 1.

The nonlinear behaviour exhibited by unidirectional layers under shear loading was introduced in the FE model by a phenomenological constitutive law (Fig. 2), which is characterised by a first stage described through a cubic polynomial stress–strain curve (reproducing the nonlinear behaviour induced by diffuse micro-cracking of the matrix), followed by a second stage represented by a linear softening law that simulates the post-failure response of the material.

Delaminations between layers of the composite skins and possible debonding between skin and core were simulated by interface cohesive elements, which enforce a constitutive law consisting of a bilinear relation between tractions and separations at the surfaces of the adjoining layers. The behaviour of the interface is linear elastic until a criterion for failure initiation is satisfied; the ensuing progressive decohesion of the interface with increasing separation is described by a linear softening phase; finally, the tractions reduce to zero and a new delaminated surface is formed when the area under the traction-separation curve equals the fracture energy of the interface. A damage indicator ranging between 0 (undamaged interface) and 1 (complete decohesion of the interface) was used to monitor the evolution of damage.

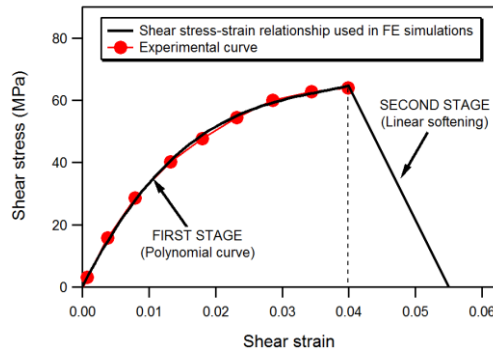


Fig. 2 Nonlinear shear stress–strain response of unidirectional layers implemented in the FE model

The stress-based quadratic criterion

$$\left(\frac{\langle t_n \rangle}{N}\right)^2 + \left(\frac{t_s}{S}\right)^2 + \left(\frac{t_t}{S}\right)^2 = 1 \quad (4)$$

was adopted in the calculations to assess the onset of the decohesion stage, while the propagation of delamination under mixed-mode loading was modelled with the power law interaction criterion

$$\left(\frac{G_I}{G_{Ic}}\right)^\delta + \left(\frac{G_{II} + G_{III}}{G_{IIc}}\right)^\beta = 1 \quad (5)$$

In the above equations, t_n , t_s , t_t represent the normal and shear interface stresses; N , S are the normal and shear interface strengths; G_{Ic} , G_{IIc} are the critical fracture energies for interlaminar fracture under normal and shear loading.

The intralaminar and interlaminar damage models were implemented into ABAQUS/Explicit through user-defined material subroutines VUMAT.

3.2 FE model of sandwich panels

The explicit commercial FE code ABAQUS/Explicit was used for simulation of the impact event. Fig. 3 shows a typical FE model of the sandwich plate built for the analyses. C3D8R solid elements were used to simulate the composite skins (with one element per layer through the thickness of the laminate) and the foam core; zero-thickness COH3D8 cohesive elements were inserted at the interfaces between layers with different fibre orientations and between skins and core to simulate delamination and core/skin debonding, respectively. The nonlinear behaviour of the foam was modelled using the crushable foam model with volumetric hardening available in ABAQUS. Elements with in-plane size of 0.5 mm by 0.5 mm were used in a finely meshed central region as visible in Fig. 3. The mesh density in this region was selected by a sensitivity analysis that showed convergence of FE solutions for element sizes smaller than about 1 mm.

The properties of the composite layers and of the foam needed by the constitutive models implemented in the FE tool (see Table 1) were obtained by a series of experimental tests expressly conducted to identify the elastic, nonlinear and fracture behaviour of the materials. In particular, fracture tests using DCB, ENF and MMB specimens were carried out to determine interlaminar fracture energies at different mixed-mode ratios. The parameters δ and β of the delamination growth criterion expressed by Eq. (5) were obtained by fitting the power law curve to the experimental fracture energy data. The values of the normal and shear interface strengths N and S in Eq. (4) were selected in a preliminary calibration phase based on the comparison of experimental results and simulations of pure mode I and mode II tests. Fibre fracture energy values G_{fi} and G_{fc} reported in the literature (Faggiani and Falzon 2010) for a different carbon/epoxy system were used in the model. Further details on materials characterization may be found in (Feng and Aymerich 2013, 2014).

The impactor and the supporting plate were modelled as rigid bodies using R3D4 rigid elements. Surface-to-surface contact pairs were defined to simulate the interaction between the panel and the surface of the impactor as well as that between the panel and the supporting plate. A mass element was used to assign a mass value of 2.34 kg to the impactor. The geometrical nonlinearity of the problem was taken into account by activating the NLGEOM option for large

deformation. Impacts of different energies were simulated by imposing the appropriate velocities of the impactor at the instant of contact with the sandwich plate.

A time increment Δt of about 5 ns was used for the explicit integration of the equilibrium equations. This time-step satisfies the stability restriction imposed by the iterative time-stepping algorithm and was selected using the element-by-element estimation scheme available in ABAQUS/Explicit, based on the evaluation of highest element frequency in the whole FE model. No mass scaling was used in the explicit analyses. All calculations were performed on a distributed-memory cluster system of three Linux workstations (each with a quad-core Intel i7-860 processor and 8 GB RAM) connected by Gigabit Ethernet, using the MPI based parallel solver available in ABAQUS/Explicit.

Table 1 Material properties used in FE analyses

Layer properties	$E_{11} = 122 \text{ GPa}; E_{22} = E_{33} = 6.2 \text{ GPa}; \nu_{12} = \nu_{13} = 0.35; \nu_{23} = 0.5;$
	$X_t = 1850 \text{ MPa}; X_c = 1470 \text{ MPa}; Y_t = 29 \text{ MPa}; Y_c = 140 \text{ MPa};$
	$G_{ft} = 92 \text{ kJ/m}^2; G_{fc} = 80 \text{ kJ/m}^2;$
	$G_{mt} = 520 \text{ J/m}^2; G_{mc} = 1610 \text{ J/m}^2$
Interface properties	$k_N = 120 \text{ GPa/mm}; k_S = k_T = 43 \text{ GPa/mm};$
	$N = 30 \text{ MPa}; S = 60 \text{ MPa};$
	$G_{IC} = 520 \text{ J/m}^2; G_{IIC} = 920 \text{ J/m}^2$

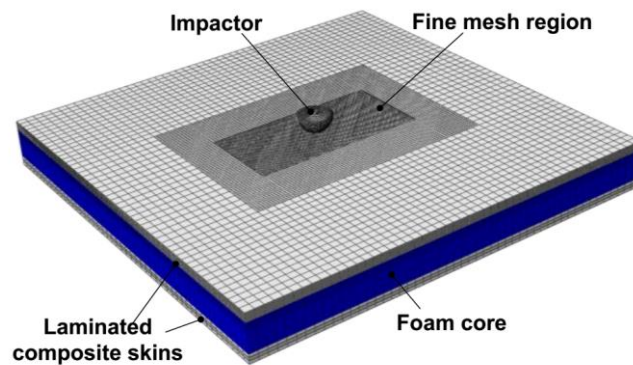


Fig. 3 FE model of sandwich panels

4. Experimental results and validation of the FE model

Typical force-time and force-displacement curves measured during impacts of about 6.2 J on sandwich panels with the three investigated skin layups are plotted in Fig. 4. As expected, mainly because of the large difference in the thickness of the skins, the structural response to impact of sandwich plates with $[0/90_3/0]$ skins is significantly different from those exhibited by panels with $[0_4/\pm 45/0_4]$ and $[0_3/\pm 45]_s$ skins. Substantial differences are for example observed in terms of impact duration, maximum force attained during the impact event and slope of the force-displacement curves, as clearly visible in the plots of Fig. 4.

Even if the force signal acquired during the impacts is disturbed, especially for high energy impacts, by inertial oscillations excited by the initial contact (Zhou *et al.* 2012), we may identify an approximately linear behaviour of the force-displacement curves up to a threshold force level (indicated by a small arrow in the plots) above which the curves exhibit an evident stiffness decrease. This threshold load level (slightly higher than 1 kN for $[0/90_3/0]$ sandwich panels and about 2 kN for $[0_4/\pm 45/0_4]$ and $[0_3/\pm 45]_s$ sandwich panels) is associated to the initiation of damage and degradation phenomena occurring in the laminated skin and in the core during the impact event.

Figs. 5-7 show typical damage patterns induced by impacts of approximately 6.2 J energy on the three classes of sandwich panels. X-ray and microscopy observations indicate that, in the range of energies investigated, impact damage in the composite skins consists mainly of a combination of tensile or shear matrix cracks and delaminations, with fibre fracture only occurring in $[0_4/\pm 45/0_4]$ and $[0_3/\pm 45]_s$ sandwich panels for impact energies higher than 6 J.

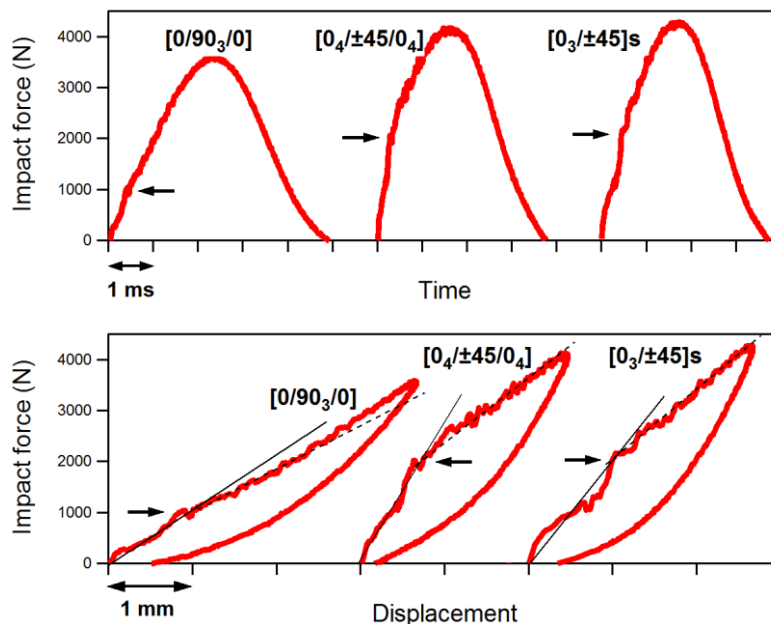


Fig. 4 Force-time and force-displacement curves of sandwich panels with $[0/90_3/0]$, $[0_4/\pm 45/0_4]$ and $[0_3/\pm 45]_s$ skins. Impact energy ≈ 6.2 J

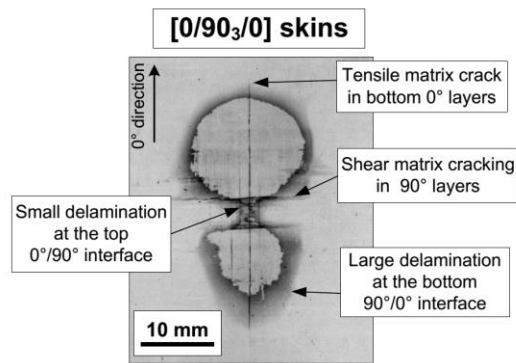


Fig. 5 X-ray of typical skin damage for sandwich panels with $[0/90_3/0]$ skins. Impact energy ≈ 6.3 J

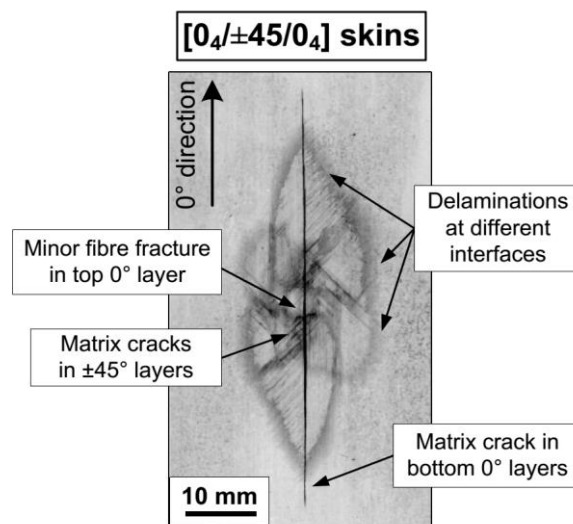


Fig. 6 X-ray of typical skin damage for sandwich panels with $[0_4/\pm 45/0_4]$ skins. Impact energy ≈ 6.2 J

Damage in the impacted skin of $[0/90_3/0]$ sandwich composites (Fig. 5) initiates at a load level lower than 1 kN, and consists of a major tensile matrix crack developing in the 0° layer adjacent to the core and of shear matrix cracking occurring in the middle 90° layers. With increasing impact energy, tensile and shear matrix cracks promote the initiation of a peanut-shape delamination on the $90^\circ/0^\circ$ interface between the cracked 0° and 90° plies (Fig. 5). Small delaminations were observed on the $0^\circ/90^\circ$ interface close to the impact side only for impact energies larger than about 6 J. No evident fibre damage was detected in the impacted facings for the entire range of impact energies investigated.

In $[0_4/\pm 45/0_4]$ and $[0_3/\pm 45]$ s sandwich panels, damage (Figs. 6 and 7) initiates at an impact

energy level of about 1 J with a large bending matrix crack developing in the lower 0° layers, followed by delamination at the $-45^\circ/+45^\circ$ and $-45^\circ/0^\circ$ interfaces and fine matrix cracking in the $+45^\circ$ and -45° plies. With increasing impact energies, delaminations tend to develop at all remaining interfaces between layers with different orientations, in association with matrix cracking in adjacent layers. In both $[0_4/\pm 45/0_4]$ and $[0_3/\pm 45]_s$ sandwich composites, fibre damage, consisting of short fibre fracture paths developing in the top 0° layers in the indentation area, is observed only for impact events with energies higher than about 6 J.

In all three sandwich configurations, collapse of the foam material in the vicinity of the impacted region, as opposed to damage in the composite layers (which is still very limited immediately after reaching the knee point of the force-displacement curves), appears as the major degradation mechanism responsible for the change in stiffness exhibited by the sandwich panels at the threshold load. It should be noted, however, that microscopy inspections on polished cross-sections of impacted sandwich panels showed no evidence of major damage phenomena within the foam (such as large cavities or fractured cell walls) or of debonding between the core and the skin, even when the sandwich panels were impacted with energies closer or higher than 8 J.

Force vs time and force vs displacement curves predicted by the FE analyses for impacts of around 2 J and 6 J are compared to experimental data in Fig. 8. It may be seen that a good agreement is achieved between experiments and simulations in terms of both force-time history and force-displacement relationship for all configurations of sandwich panels investigated. In particular, the model is able to capture with excellent accuracy not only the peak force values and the durations of the impact event, but also the characteristic nonlinearities, such as the drastic stiffness change occurring above the threshold load (indicated by small arrows in the plots) and the different shapes of the loading and unloading stages, typical of the force-displacement response to impact of the three sandwich configurations.

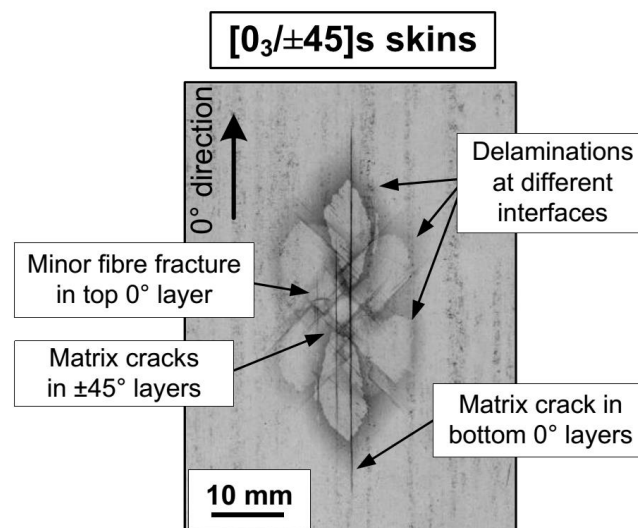


Fig. 7 X-ray of typical skin damage for a sandwich panels with $[0_3/\pm 45]_s$ skins. Impact energy ≈ 6.2 J

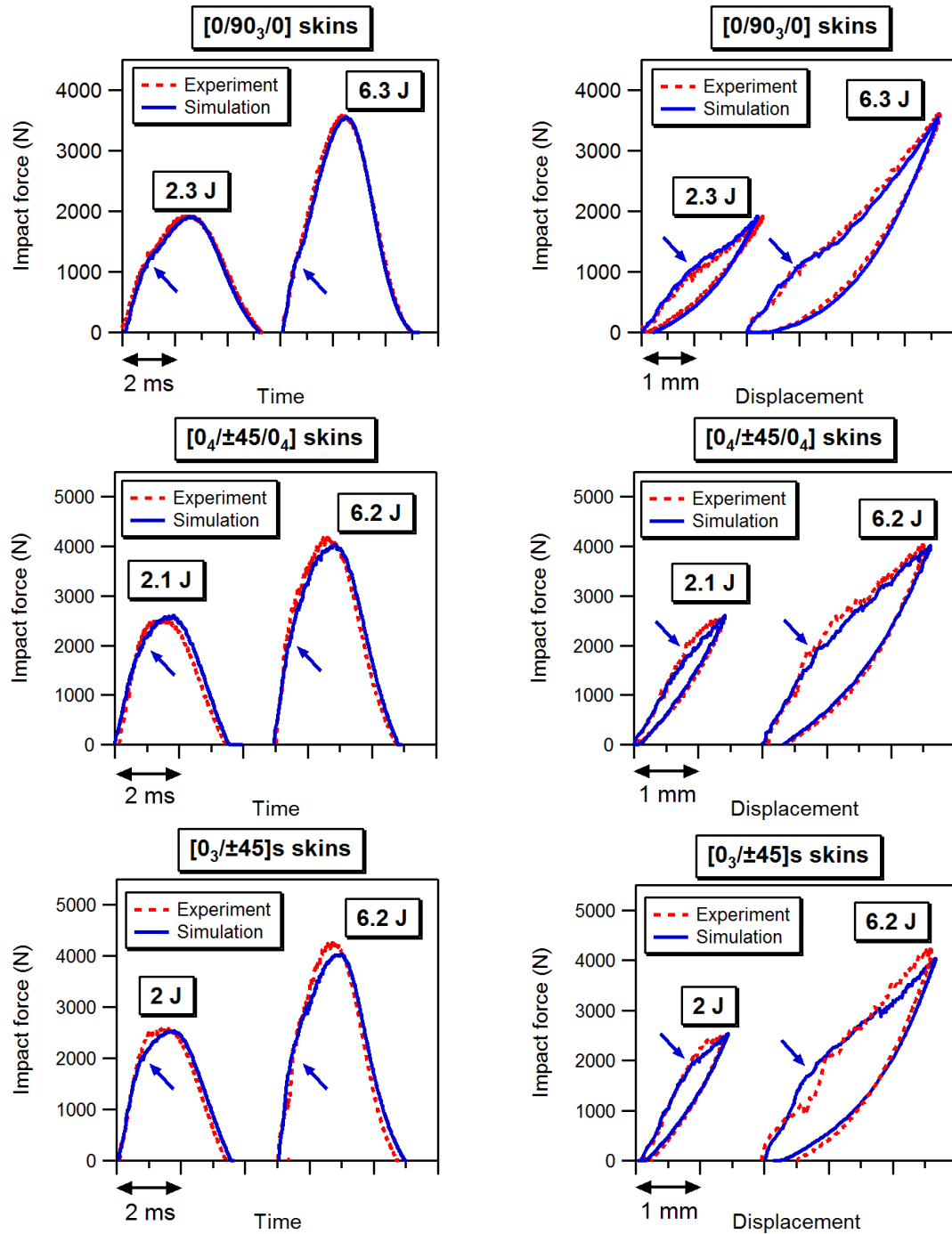


Fig. 8 Comparison between experimental and simulated force–time histories (left column) and force–displacement curves (right column) for sandwich panels with $[0/90_3/0]$, $[0_4/\pm 45/0_4]$ and $[0_3/\pm 45]_s$ skins impacted at two energy levels

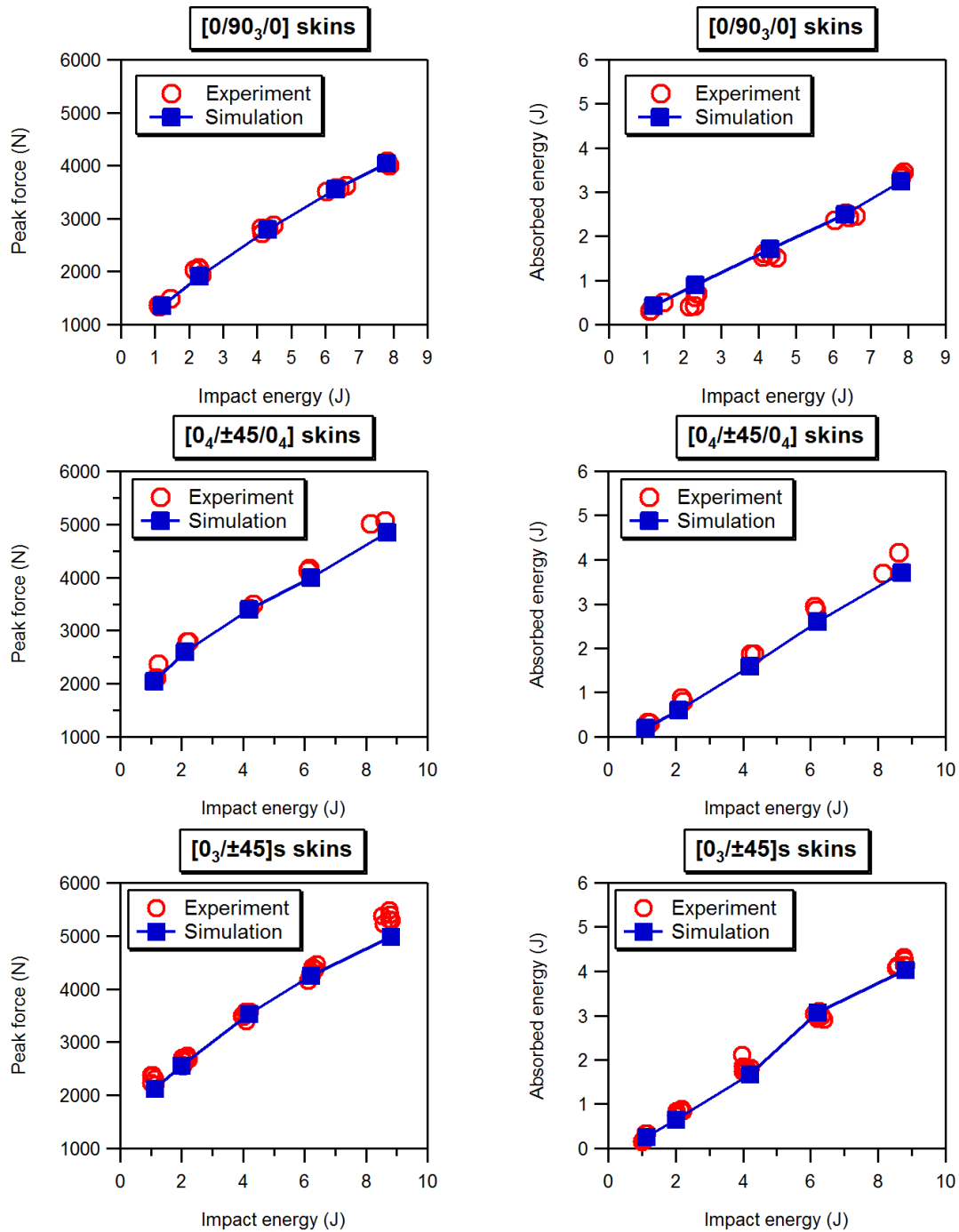


Fig. 9 Comparison between experimental and predicted peak contact forces (left column) and absorbed energies (right column) for sandwich panels with [0/90₃/0], [0₄/±45/0₄] and [0₃/±45]s skins

Quantitative comparisons of predicted and measured peak contact forces and absorbed energies are shown in Fig. 9. The predicted values of the absorbed energy plotted in the graphs are calculated as the area under the force-displacement curve, which represents the total energy dissipated during the impact in irreversible damage mechanisms (foam nonlinearities, intralaminar or interlaminar fracture in the impacted skins, plastic deformation in the composite layers, etc.). The graphs show that there is a rather good correlation between numerical predictions and experimental data, with only a slight tendency of the FE model to underpredict the maximum force values at high impact energies for impacts on $[0_4/\pm 45/0_4]$ and $[0_3/\pm 45]$ s sandwich plates. Since fibre fractures are only observed on sandwich panels with $[0_4/\pm 45/0_4]$ and $[0_3/\pm 45]$ s skins, and not on $[0/90_3/0]$ sandwich panels, this small discrepancy may be attributed to the use in the model of fibre fracture energy values determined from tests on a different carbon/epoxy material.

The values of the projected damage areas induced by impact on the composite skins are plotted versus impact energy in the graphs of Fig. 10. The comparisons show that the FE simulations predict with reasonable accuracy the trend of damage area growth with increasing impact energy for all sandwich configurations.

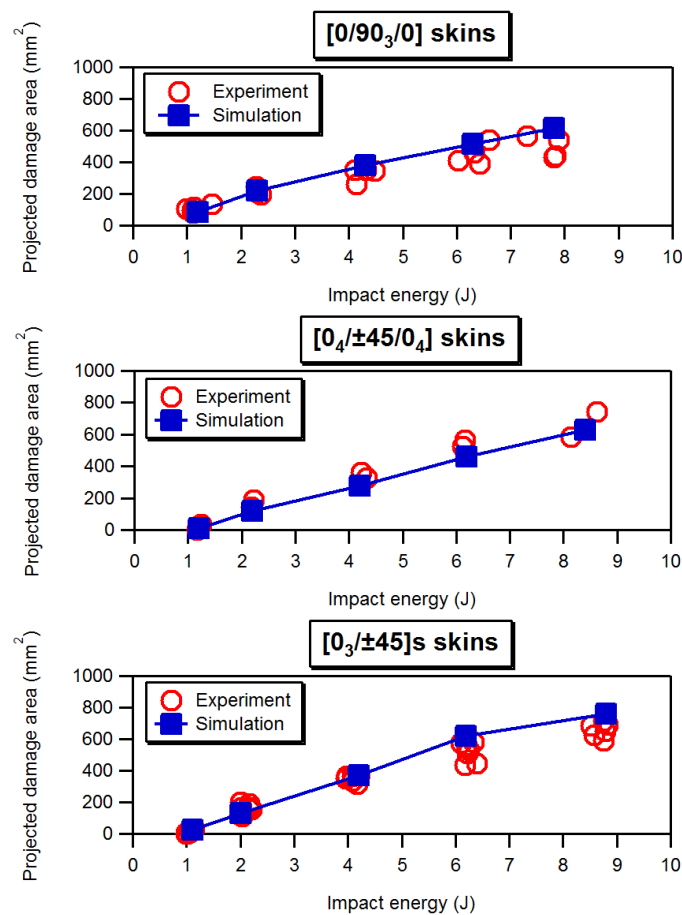


Fig. 10 Comparison between projected damage areas as obtained by X-ray and predicted by the FE model for sandwich panels with $[0/90_3/0]$, $[0_4/\pm 45/0_4]$ and $[0_3/\pm 45]$ s skins impacted at various energies

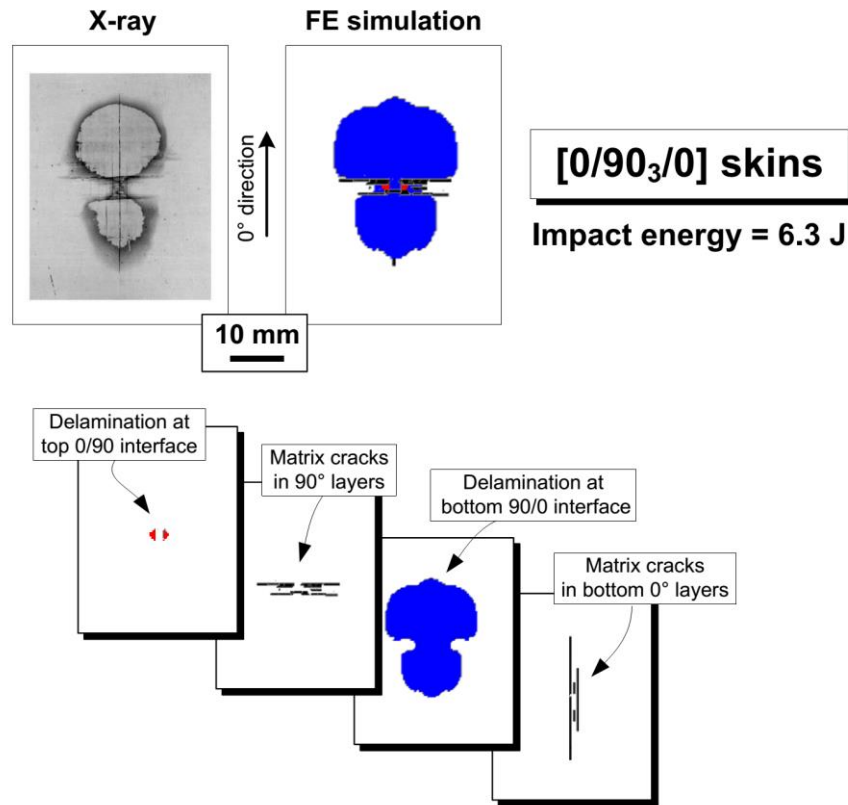


Fig. 11 Comparison of projected damage and through-thickness distribution of individual damage modes as obtained by X-ray and predicted by the FE model for a sandwich panel with $[0/90_3/0]$ skins. Impact energy ≈ 6.3 J

Images of impact damage as obtained by X-radiography and predicted by FE simulations (where different colours correspond to different delamination depths) are shown in Figs. 11-13. Experimental and predicted damage patterns for an impact of 6.3 J on a sandwich composite with $[0/90_3/0]$ skins are compared in Fig. 11. It is seen that the FE simulations provide a good prediction of the global shape and of the typical features that characterize the damage scenario of the examined sandwich configurations. In particular, the FE model is capable of successfully predicting the individual damage mechanisms that develop at various through-thickness depths in the different composite lay-ups. As visible in Fig. 11, the simulation successfully captures the development of a long matrix crack in the lower 0° layers, the presence of shear matrix cracking in the 90° layers around the impact axis, and the onset and growth of a large two-lobe delamination on the bottom $90^\circ/0^\circ$ interface of the laminated skin of $[0/90_3/0]$ sandwich panels.

Figs. 12 and 13 show that the model is also able to properly simulate the damage pattern of $[0_4/\pm 45/0_4]$ and $[0_3/\pm 45]$ s sandwich panels, by successfully reproducing the general shape of the projected damage areas, with their major axis elongated along the 0° direction, and identifying correctly the shape, orientation and location of individual delaminated areas at different interfaces.

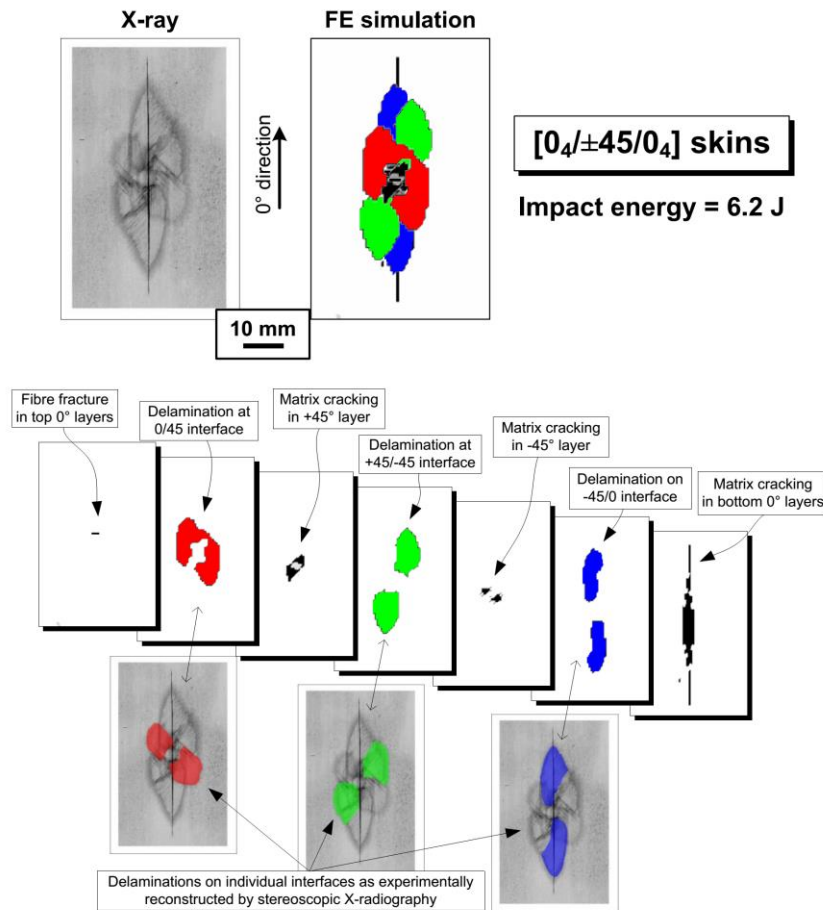


Fig. 12 Comparison of projected damage and through-thickness distribution of individual damage modes as obtained by X-ray and predicted by the FE model for a sandwich panel with $[0_4/\pm 45/0_4]$ skins. Impact energy ≈ 6.2 J

As an example, a detailed illustration of the damage scenario predicted by the FE model through the thickness of the laminated skin of a $[0_4/\pm 45/0_4]$ sandwich panel subjected to a 6.2 J impact is shown in Fig. 12 in comparison to delaminated areas at the various interfaces as identified by X-ray stereoscopy and confirmed by ultrasonics. FE predictions of internal damage, which is mainly characterized by three large delaminations at the interfaces between different layer orientations, are in reasonably good agreement with the actual impact damage features. In accordance with experimental observations, it is seen, in particular, that delaminations simulated at specific interfaces have a characteristic peanut-like shape, with the elongated portion aligned with the fibre direction of the lower ply of the interface and with a section that reduces toward the impact axis. Other key features of the damage, including the long central matrix crack in the bottom 0° layers, diffuse matrix cracking in the $\pm 45^\circ$ layers, and minor fibre fracture at the contact area in the top 0° layers are also correctly simulated by the FE model.

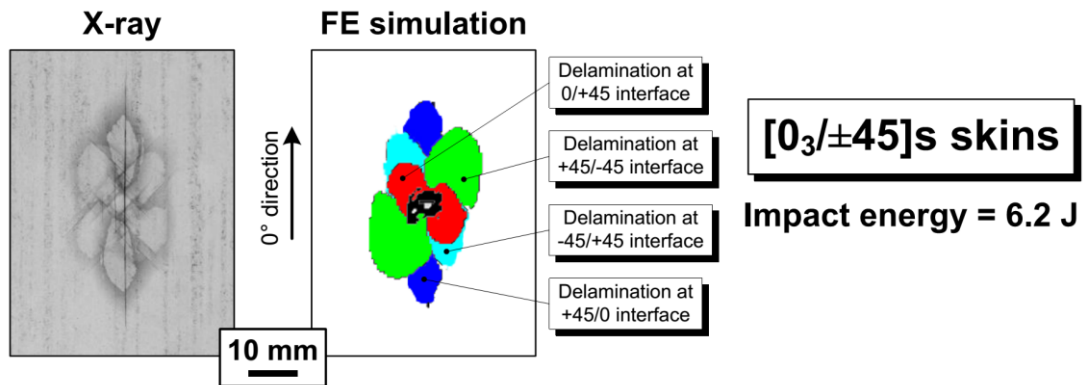


Fig. 13 Comparison of projected damage as obtained by X-ray and predicted by the FE model for a sandwich panel with $[0_3/\pm 45]_s$ skins. Impact energy ≈ 6.2 J. Different colours of the FE simulation correspond to different damage depths

The comparison between experimental and numerically simulated damage maps for a 6.2 J impact on a sandwich panel with $[0_3/\pm 45]_s$ skins, illustrated in Fig. 13, shows that the FE simulations predict the development of interlaminar damage at all four delamination-prone interfaces. The numerical reconstruction of internal damage confirms the accuracy of the damage predictions provided by the FE model, which again shows the capability to provide a reliable three-dimensional simulation of the internal damage even in the presence of complex damage scenarios, characterised by the presence of many overlapping delaminations and different interacting damage mechanisms.

5. Conclusions

The paper illustrates the application of an FE tool developed by the authors for the numerical simulation of the structural response and the damage resistance of foam-based sandwich composites subjected to low-velocity impact. Sandwich panels with PVC foam core and carbon/epoxy skins with different layups ($[0/90_3/0]$, $[0_4/\pm 45/0_4]$ and $[0_3/\pm 45]_s$) were manufactured and subjected to low-velocity impact at various BVID impact energies. The damage inflicted by impact on the three skin layups was characterised by different patterns and levels of complexity, and provided a suitable experimental background for testing the predictive capabilities of the proposed FE tool. The results of the FE simulations were compared with experimental data acquired during the impact tests and with pictures of internal damage reconstructed by X-ray analyses for the various sandwich configurations.

The comparisons show that the FE tool is able to accurately predict force-time histories, force-displacement curves and energies absorbed during impact over the entire range of examined impact energies. Moreover, the FE simulations correctly capture the planar extent of the damage area as well as the typical features of the individual interlaminar and intralaminar damage mechanisms, such as delaminations, matrix cracking and fibre fracture, occurring at different depths of the three composite skin layups. The findings of this study indicate that appropriate FE

tools can yield accurate and detailed simulations of the impact damage response of sandwich composites, thus providing valuable information for damage tolerant design of structural elements based on complex sandwich configurations. Further investigations are however required to assess the accuracy of the model predictions for different loading conditions and structural configurations (i.e. for different structure sizes or geometries, impactor shapes, boundary conditions, strain rates, etc.) and in the presence of more severe fibre-dominated damage scenarios.

Acknowledgments

The research described in this paper was financially supported by the EU funded FP7-ITN-Marie Curie project SYSWIND (Grant No. FP7-PEOPLE-ITN 238325).

References

- Abrate, S. (1997), "Localized impact on sandwich structures with laminated facings", *Appl. Mech. Rev.*, **50**, 69-97.
- Berggreen C., Branner K., Jensen J.F. and Schultz, J.P. (2007), "Application and analysis of sandwich elements in the primary structure of large wind turbine blades", *J. Sandw. Struct. Mater.*, **9**(6), 525-552.
- Besant, T., Davies, G.A.O. and Hitchings D. (2001), "Finite element modelling of low velocity impact of composite sandwich panels", *Compos. part A - Appl. S.*, **32**(9), 1189-1196.
- Brøndsted, P. and Nijssen, R.P.L. (2013), *Advances in Wind Turbine Blade Design and Materials*, Woodhead Publishing Limited, Cambridge, UK.
- Brooks, R., Brown, K.A., Warrior, N.A. and Kulandaivel, P.P. (2010), "Predictive modeling of the impact response of thermoplastic composite sandwich structures", *J. Sandw. Struct. Mater.*, **12**(4), 449-476.
- Burton, T., Jenkins, N., Sharpe, D. and Bossanyi, E. (2011), *Wind Energy Handbook*, 2nd Ed., John Wiley & Sons, Ltd, Chichester, UK.
- Chai, G.B. and Zhu S. (2011), "A review of low-velocity impact on sandwich structures", *Proc. Inst. Mech. Eng. Part L J. Mater. Des. Appl.*, **225**(4), 207-230.
- Det Norske Veritas (2006), *Design And Manufacture of Wind Turbine Blades - Offshore and Onshore Wind Turbines*, DNV-OS-J102.
- Det Norske Veritas and Risø National Laboratory (2002), *Guidelines for Design of Wind Turbine*, 2nd edition.
- Donadon, M.V., Iannucci, L., Falzon, B.G., Hodgkinson, J.M. and de Almeida, S.F.M. (2008), "A progressive failure model for composite laminates subjected to low velocity impact damage", *Comput. Struct.*, **86**(11-12), 1232-1252.
- Faggiani, A. and Falzon, B.G. (2010), "Predicting low-velocity impact damage on a stiffened composite panel", *Compos. part A-Appl. S.*, **41**(6), 737-749.
- Falzon, B.G. and Apruzzese, P. (2011), "Numerical analysis of intralaminar failure mechanisms in composite structures. Part I: FE implementation", *Compos. Struct.*, **93**(2), 1039-1046.
- Feng, D. and Aymerich, F. (2013), "Damage prediction in composite sandwich panels subjected to low-velocity impact", *Compos. part A-Appl. S.*, **52**, 12-22.
- Feng, D. and Aymerich, F. (2014), "Finite element modelling of damage induced by low-velocity impact on composite laminates", *Compos. Struct.*, **108**, 161-171.
- Hayman, B. (2007), "Approaches to damage assessment and damage tolerance for FRP sandwich structures", *J. Sandw. Struct. Mater.*, **9**(6), 571-595.
- Hayman, B., Wedel-Heinen, J. and Brøndsted P. (2008), "Materials challenges in present and future wind energy", *MRS Bulletin*, **33**, 343-353.

- Icardi, U. and Ferrero, L. (2009), "Impact analysis of sandwich composites based on a refined plate element with strain energy updating", *Compos. Struct.*, **89**(1), 35-51.
- Ivanez, I., Santiuste, C. and Sanchez-Saez, S. (2010), "FEM analysis of dynamic flexural behaviour of composite sandwich beams with foam core", *Compos. Struct.*, **92**(9), 2285-2291.
- Langdon, G.S., Karagiozova, D., von Klemperer C.J., Nurick, G.N., Ozinski, A. and Pickering, E.G. (2013), "The air-blast response of sandwich panels with composite face sheets and polymer foam cores: Experiments and predictions", *Int. J. Impact Eng.*, **54**, 64-82.
- Mohammed, R., Zhang, F., Sun, B. and Gu, B. (2013), "Finite element analyses of low-velocity impact damage of foam sandwiched composites with different ply angles face sheets", *Mater. Design*, **47**, 189-199.
- Nguyen, M.Q., Jacombs, S.S., Thomson, R.S., Hachenberg, D. and Scott, M.L. (2005), "Simulation of impact on sandwich structures", *Compos. Struct.*, **67**(2), 217-227.
- Ransom, J.B., Glaessgen, E.H., Raju, I.S. and Harris, C.E. (2013), "Recent advances in durability and damage tolerance methodology at NASA Langley Research Center", in *Advances in Interdisciplinary Mathematical Research*, Bourama Toni, Ed., Springer, New York.
- Schurmann, H. and Puck, A. (2002), "Failure analysis of FRP laminates by means of physically based phenomenological models", *Compos. Sci. Technol.*, **62**, 1633-1662.
- Thomsen, O.T. (2009), "Sandwich materials for wind turbine blades - present and future", *J Sandw. Struct. Mater.*, **11**(1), 7-26.
- Wang, J., Waas A.M. and Wang H. (2013), "Experimental and numerical study on the low-velocity impact behavior of foam-core sandwich panels", *Compos. Struct.*, **96**, 298-311.
- Yang, P., Shams, S.S., Slay, A., Brokate, B. and Elhajjar, R. (2015), "Evaluation of temperature effects on low velocity impact damage in composite sandwich panels with polymeric foam cores", *Compos. Struct.*, **129**, 213-223.
- Zenkert, D., Shipsha, A., Bull, P. and Hayman, B. (2005), "Damage tolerance assessment of composite sandwich panels with localised damage", *Compos. Sci. Technol.*, **65**(15), 2597-2611.
- Zhou, J., Hassan, M.Z., Guan, Z. and Cantwell, W.J. (2012), "The low velocity impact response of foam-based sandwich panels", *Compos. Sci. Technol.*, **72**(14), 1781-1790.